ACADEMIC PRESS

Available online at www.sciencedirect.com

SCIENCE DIRECT®

Journal of Sound and Vibration 270 (2004) 847–863

JOURNAL OF SOUND AND VIBRATION

www.elsevier.com/locate/jsvi

Non-linear dynamic analysis of beams with variable stiffness

J.T. Katsikadelis*, G.C. Tsiatas

Department of Civil Engineering, National Technical University of Athens, Zografou Campus, GR-15773 Athens, Greece

Received 8 July 2002; accepted 28 January 2003

Abstract

In this paper the analog equation method (AEM), a BEM-based method, is employed to the non-linear dynamic analysis of a Bernoulli–Euler beam with variable stiffness undergoing large deflections, under general boundary conditions which maybe non-linear. As the cross-sectional properties of the beam vary along its axis, the coefficients of the differential equations governing the dynamic equilibrium of the beam are variable. The formulation is in terms of the displacements. The governing equations are derived in both deformed and undeformed configuration and the deviations of the two approaches are studied. Using the concept of the analog equation, the two coupled non-linear hyperbolic differential equations with variable coefficients are replaced by two uncoupled linear ones pertaining to the axial and transverse deformation of a substitute beam with unit axial and bending stiffness, respectively, under fictitious time-dependent load distributions. A significant advantage of this method is that the time history of the displacements as well as the stress resultants are computed at any cross-section of the beam using the respective integral representations as mathematical formulae. Beams with constant and varying stiffness are analyzed under various boundary conditions and loadings to illustrate the merits of the method as well as its applicability, efficiency and accuracy.

1. Introduction

In recent years a need has been raised in engineering practice to predict accurately the non-linear response of beams subjected to dynamic loads, especially when the properties of their cross-section are variable. The non-linearity results from retaining the square of the slope in the strain–displacement relations (intermediate non-linear theory). In this case the transverse deflection influences the axial force and the resulting equations, governing the dynamic response of the beam, are coupled non-linear with variable coefficients. Moreover, the pertinent boundary conditions of the problem are in general non-linear.

*Corresponding author. Tel.: +30-772-1654; fax: +30-772-1655.
E-mail address: jkats@central.ntua.gr (J.T. Katsikadelis).

0022-460X/$ - see front matter © 2003 Elsevier Ltd. All rights reserved.
doi:10.1016/S0022-460X(03)00635-7

Many researchers have been involved in the solution of the problem using various techniques. In all cases only axially immovable supports have been considered. Approximate analytical solutions are restricted only to large-amplitude free vibration of uniform beams [1–4] using elliptic integrals, perturbation or Ritz–Galerkin methods. The Galerkin method has also been used by Raju et al. [5] to analyze the large-amplitude free vibrations of tapered beams, while Sato [6] investigated the non-linear free vibrations of stepped height beams using the transfer matrix method. Numerical methods have been developed for the solution of the problem like the finite difference method [7]. The finite element method was used for free non-linear vibrations of uniform beams [8,9] and of tapered beams [10] as well as for forced non-linear vibrations of uniform beams [11–14].

The complexity of the problem compelled many of the above researchers to make gross simplifications in addition to considering the equilibrium in the undeformed configuration. In the case of non-linear free vibrations [1–6,8–10] either the time function or the space function is assumed and a characteristic non-linear frequency is computed. Although this is correct in the linear vibration theory, the non-linear free vibration problem does not admit this separation since the mode shape varies also with time. The FEM has been successfully employed to the solution of forced non-linear vibrations of beams with constant cross-section [11–14]. However, beams with non-uniform cross-section are often approximated by a large number of small uniform elements replacing the continuous variation with a step law. In this way it is always possible to obtain acceptable results and the error can be reduced as much as desired by refining the mesh, at the expense of computational cost.

In this paper, an accurate direct solution to the governing coupled non-linear differential equations of hyperbolic type is presented, which permits the treatment also of non-linear boundary conditions. The governing equations are derived in both deformed and undeformed configuration. The solution method is based on the concept of the analog equation [15]. According to this, the two coupled non-linear differential equations are replaced by two equivalent uncoupled linear ones pertaining to the axial and transverse deformation of a substitute beam with unit axial and bending stiffness subjected to fictitious time-dependent load distributions under the same boundary conditions. Several beams are analyzed under various boundary conditions and load distributions, which illustrate the method and demonstrate its efficiency and accuracy. Moreover, useful conclusions are drawn from the comparison of the two sets of equations referred to deformed and undeformed configuration. The latter one is usually adopted in the literature to reduce the non-linearity of the problem.

2. Governing equations

Consider an initially straight beam of length l having variable axial EA and bending stiffness EI, which may result from variable cross-section, $A = A(x)$, and/or from inhomogeneous linearly elastic material, $E = E(x)$; $I = I(x)$ is the moment of inertia of the cross-section. The x-axis coincides with the neutral axis of the beam, which is bent in its plane of symmetry xz under the combined action of the distributed loads $p_x = p_x(x)$ and $p_z = p_z(x, t)$ in the x and z direction respectively. The large deflection theory result from the non-linear kinematic relation, which retains the square of the slope of the deflection, while the strain component remains still small

compared with the unity. Therefore

$$\varepsilon_x(x,z) = u_{,x} + \tfrac{1}{2} w_{,x}^2 + z\kappa, \tag{1}$$

where $u = u(x,t)$ and $w = w(x,t)$ are displacements along the x- and z-axis, respectively, and κ is the curvature of the deflected axis.

Referring to the equilibrium of the deformed element (see Fig. 1) the following relations are derived:

$$p_x^* = p_x \, \mathrm{d}x/\mathrm{d}s, \quad p_z^* = p_z \, \mathrm{d}x/\mathrm{d}s, \tag{2,3}$$

$$\mathrm{d}s = \sqrt{(1+u_{,x})^2 + w_{,x}^2}\, \mathrm{d}x, \tag{4}$$

$$\cos\theta = \frac{1+u_{,x}}{\sqrt{(1+u_{,x})^2 + w_{,x}^2}}, \quad \sin\theta = \frac{w_{,x}}{\sqrt{(1+u_{,x})^2 + w_{,x}^2}}, \tag{5,6}$$

which for the case of moderate large deflections ($u_{,x}, w_{,x}^2 \ll 1$) become

$$p_x^* = p_x, \quad p_z^* = p_z, \tag{7,8}$$

$$\mathrm{d}s = \mathrm{d}x, \tag{9}$$

$$\cos\theta \simeq 1, \quad \sin\theta \simeq w_{,x} \simeq \theta. \tag{10,11}$$

Moreover, the strain $\varepsilon_0 = \varepsilon_x(x,0)$ at the x-axis and the curvature $\kappa = \kappa(x)$ are given as

$$\varepsilon_0 = u_{,x} + \tfrac{1}{2} w_{,x}^2, \tag{12}$$

$$\kappa = \frac{\mathrm{d}\theta}{\mathrm{d}s} \simeq \theta_{,x} \simeq w_{,xx}. \tag{13}$$

Therefore, the stress resultants, that is the axial force and the bending moment are given as

$$N = EA(u_{,x} + \tfrac{1}{2} w_{,x}^2), \tag{14}$$

$$M = -EIw_{,xx}. \tag{15}$$

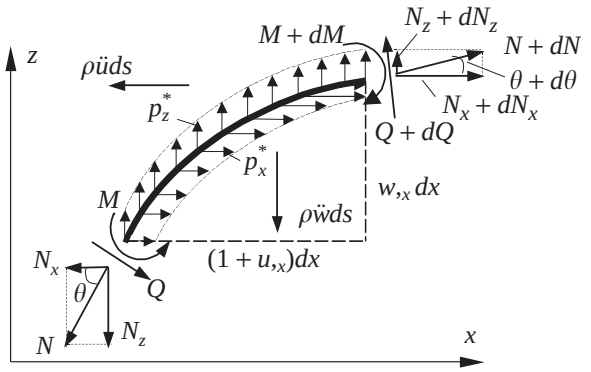

Fig. 1. Forces and moments acting on the deformed element.

From Fig. 1,

$$N_x = N\cos\theta - Q\sin\theta \simeq N - Qw_{,x}, \tag{16}$$

$$N_z = N\sin\theta + Q\cos\theta \simeq Nw_{,x} + Q. \tag{17}$$

The equations of motion are derived by considering the equilibrium of the deformed element. Thus, referring to Fig. 1 one obtains

$$-\rho\ddot{u} + N_{x,x} = -p_x, \tag{18}$$

$$-\rho\ddot{w} + N_{z,x} = -p_z, \tag{19}$$

$$M_{,x} = Q, \tag{20}$$

where $\rho = \rho(x)$ is the mass density per unit length.

Substituting Eqs. (16) and (17) into Eqs. (18) and (19) and using Eq. (20) to eliminate Q, gives

$$-\rho\ddot{u} + N_{,x} - (M_{,x}w_{,x})_{,x} = -p_x, \tag{21}$$

$$-\rho\ddot{w} + M_{,xx} + (Nw_{,x})_{,x} = -p_z, \tag{22}$$

which by virtue of Eqs. (14) and (15) become

$$-\rho\ddot{u} + [EA(u_{,x} + \tfrac{1}{2}w_{,x}^2)]_{,x} + (EIw_{,xxx}w_{,x})_{,x} = -p_x, \tag{23}$$

$$-\rho\ddot{w} - (EIw_{,xx})_{,xx} + [EA(u_{,x} + \tfrac{1}{2}w_{,x}^2)w_{,x}]_{,x} = -p_z. \tag{24}$$

The pertinent boundary conditions are

$$a_1u(0,t) + a_2N_x(0,t) = a_3 \quad \text{and} \quad \bar{a}_1u(l,t) + \bar{a}_2N_x(l,t) = \bar{a}_3, \tag{25, 26}$$

$$\beta_1w(0,t) + \beta_2N_z(0,t) = \beta_3 \quad \text{and} \quad \bar{\beta}_1w(l,t) + \bar{\beta}_2N_z(l,t) = \bar{\beta}_3, \tag{27, 28}$$

$$\gamma_1w_{,x}(0,t) + \gamma_2M(0,t) = \gamma_3 \quad \text{and} \quad \bar{\gamma}_1w_{,x}(l,t) + \bar{\gamma}_2M(l,t) = \bar{\gamma}_3, \tag{29, 30}$$

and the initial conditions are

$$u(x,0) = \tilde{u}(x), \quad \dot{u}(x,0) = \dot{\tilde{u}}(x), \tag{31, 32}$$

$$w(x,0) = \tilde{w}(x), \quad \dot{w}(x,0) = \dot{\tilde{w}}(x), \tag{33, 34}$$

where a_k, $\bar{a}_k$, β_k, $\bar{\beta}_k$, γ_k, $\bar{\gamma}_k$ $(k = 1, 2, 3)$ are given constants and $\tilde{u}(x)$, $\dot{\tilde{u}}(x)$, $\tilde{w}(x)$, $\dot{\tilde{w}}(x)$ are prescribed functions. For example at an end restrained elastically in the x direction, say at $x = 0$, the boundary condition (25) becomes, $k_xu(0,t) + N_x(0,t) = P_x$, that is $a_1 = k_x$, $a_2 = 1$ and $a_3 = P_x$; k_x is the stiffness of the spring and P_x the external applied force. The boundary conditions (29) and (30) are linear. However, on the basis of Eqs. (16) and (17) the boundary conditions (25)–(28) are, in general, non-linear.

The term $Qw_{,x} = EIw_{,xxx}w_{,x}$, which appears in Eq. (23), expresses the influence of the shear force Q on N_x. The presence of this term increases highly the difficulty of the solution. The existing solutions circumvent this difficulty by neglecting this non-linear term. This assumption yields $N_x \simeq N$ and it is true if the equilibrium is considered in the undeformed configuration. Thus

the governing equations are simplified as

$$-\rho\ddot{u} + [EA(u_{,x} + \tfrac{1}{2}w_{,x}^2)]_{,x} = -p_x, \tag{35}$$

$$-\rho\ddot{w} - (EIw_{,xx})_{,xx} + [EA(u_{,x} + \tfrac{1}{2}w_{,x}^2)w_{,x}]_{,x} = -p_z, \tag{36}$$

while the boundary conditions become

$$a_1u(0,t) + a_2N(0,t) = a_3 \quad \text{and} \quad \bar{a}_1u(l,t) + \bar{a}_2N(l,t) = \bar{a}_3, \tag{37,38}$$

$$\beta_1w(0,t) + \beta_2N_z(0,t) = \beta_3 \quad \text{and} \quad \bar{\beta}_1w(l,t) + \bar{\beta}_2N_z(l,t) = \bar{\beta}_3, \tag{39,40}$$

$$\gamma_1w_{,x}(0,t) + \gamma_2M(0,t) = \gamma_3 \quad \text{and} \quad \bar{\gamma}_1w_{,x}(l,t) + \bar{\gamma}_2M(l,t) = \bar{\gamma}_3. \tag{41,42}$$

The validity of this simplifying assumption is investigated by solving both sets of governing equations and useful conclusions are drawn.

3. The AEM solution

Eqs. (23) and (24) are solved using the AEM, which for the problem at hand is applied as follows. Let $u = u(x,t)$ and $w = w(x,t)$ be the sought solutions, which are two and four times differentiable, respectively, in $(0,l)$. Noting that Eqs. (23) and (24) are of the second order with respect to u, of fourth order with respect to w, one obtains by differentiating

$$u_{,xx} = b_1(x,t), \tag{43}$$

$$w_{,xxxx} = b_2(x,t), \tag{44}$$

where b_1, b_2 are fictitious loads depending also on time. Eqs. (43) and (44) indicate that the solution of Eqs. (23) and (24) can be established by solving Eqs. (43) and (44) under the boundary conditions (25)–(30), provided that the fictitious load distributions b_1, b_2 are first determined. Note that Eqs. (23) and (24) are quasi-static, that is the time is considered as a parameter.

The fictitious loads are established by developing a procedure based on the boundary integral equation method for one-dimensional problems. Thus, the integral representations of the solutions of Eqs. (43) and (44) are written as

$$u(x,t) = c_1x + c_2 + \int_0^l G_1(x,\xi)b_1(\xi,t)\,\mathrm{d}\xi, \tag{45}$$

$$w(x,t) = c_3x^3 + c_4x^2 + c_5x + c_6 + \int_0^l G_2(x,\xi)b_2(\xi,t)\,\mathrm{d}\xi, \tag{46}$$

where $c_i = c_i(t)$ $(i = 1,2,\ldots,6)$ are arbitrary time-dependent integration functions to be determined from the boundary conditions and $G_i(x,\xi)$ $(i = 1,2)$ are the fundamental solutions of Eqs. (43) and (44), that is a particular singular solution of the following equations:

$$G_{1,xx} = \delta(x-\xi), \tag{47}$$

$$G_{2,xxxx} = \delta(x-\xi), \tag{48}$$

with $\delta(x-\xi)$ being the Dirac function.

Integration of Eqs. (47) and (48) yields

$$G_1 = \tfrac{1}{2}|x-\xi|, \tag{49}$$

$$G_2 = \tfrac{1}{12}|x-\xi|(x-\xi)^2. \tag{50}$$

The derivatives of u and w are obtained by direct differentiation of Eqs. (45) and (46). Thus,

$$u_{,x}(x,t) = c_1 + \int_0^l G_{1,x}(x,\xi)b_1(\xi,t)\,\mathrm{d}\xi, \tag{51}$$

$$u_{,xx}(x,t) = b_1(x,t), \tag{52}$$

$$w_{,x}(x,t) = 3c_3x^2 + 2c_4x + c_5 + \int_0^l G_{2,x}(x,\xi)b_2(\xi,t)\,\mathrm{d}\xi, \tag{53}$$

$$w_{,xx}(x,t) = 6c_3x + 2c_4 + \int_0^l G_{2,xx}(x,\xi)b_2(\xi,t)\,\mathrm{d}\xi, \tag{54}$$

$$w_{,xxx}(x,t) = 6c_3 + \int_0^l G_{2,xxx}(x,\xi)b_2(\xi,t)\,\mathrm{d}\xi, \tag{55}$$

$$w_{,xxxx}(x,t) = b_2(x,t). \tag{56}$$

Substituting the derivatives in Eqs. (23) and (24) yields the equations, from which the fictitious sources b_1 and b_2 can be determined. This can be implemented only numerically as follows.

The interval $(0,l)$ is divided into N equal elements, having length l/N. Thus, the integral equations (45) and (46) are written as

$$u(x,t) = c_1x + c_2 + \sum_{j=1}^{N} \int_j G_1(x,\xi)b_1(\xi,t)\,\mathrm{d}\xi, \tag{57}$$

$$w(x,t) = c_3x^3 + c_4x^2 + c_5x + c_6 + \sum_{j=1}^{N} \int_j G_2(x,\xi)b_2(\xi,t)\,\mathrm{d}\xi, \tag{58}$$

where the symbol $\int_j$ indicates the integral on the j-element. Subsequently, the fictitious sources are approximated on each integration interval using constant, linear or quadratic variation. In this investigation, the constant element is employed. That is, the fictitious source is assumed constant on the element and its nodal value is placed at the midpoint of the element as illustrated in Fig. 2. The integration of the kernels is performed analytically.

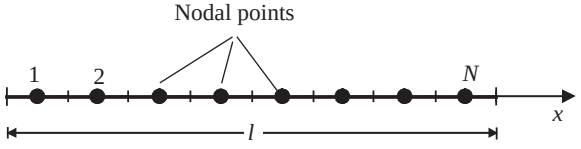

Fig. 2. Discritization of the interval and distribution of the nodal points.

Using this discretization and applying equations (51)–(58) to the N nodal points, one obtains

$$\mathbf{u} = c_1\mathbf{x}_1 + c_2\mathbf{x}_0 + \mathbf{G_1}\mathbf{b}_1, \tag{59}$$

$$\mathbf{u}_{,\mathbf{x}} = c_1\mathbf{x}_0 + \mathbf{G_{1,x}}\mathbf{b}_1, \tag{60}$$

$$\mathbf{u}_{,\mathbf{xx}} = \mathbf{b}_1, \tag{61}$$

$$\mathbf{w} = c_3\mathbf{x}_3 + c_4\mathbf{x}_2 + c_5\mathbf{x}_1 + c_6\mathbf{x}_0 + \mathbf{G_2}\mathbf{b}_2, \tag{62}$$

$$\mathbf{w}_{,\mathbf{x}} = 3c_3\mathbf{x}_2 + 2c_4\mathbf{x}_1 + c_5\mathbf{x}_0 + \mathbf{G_{2,x}}\mathbf{b}_2, \tag{63}$$

$$\mathbf{w}_{,\mathbf{xx}} = 6c_3\mathbf{x}_1 + 2c_4\mathbf{x}_0 + \mathbf{G_{2,xx}}\mathbf{b}_2, \tag{64}$$

$$\mathbf{w}_{,\mathbf{xxx}} = 6c_3\mathbf{x}_0 + \mathbf{G_{2,xxx}}\mathbf{b}_2, \tag{65}$$

$$\mathbf{w}_{,\mathbf{xxxx}} = \mathbf{b}_2, \tag{66}$$

where $\mathbf{G_1}, \mathbf{G_{1,x}}, \ldots, \mathbf{G_{2,xxx}}$ are $(N \times N)$ known matrices, originating from the integration of the kernels $G_1(x,\xi)$, $G_2(x,\xi)$ and their derivatives on the elements; $\mathbf{u}, \mathbf{u}_{,\mathbf{x}}, \ldots, \mathbf{w}_{,\mathbf{xxxx}}$ are $(N \times 1)$ vectors including the values of u, w and their derivatives at the nodal points; $\mathbf{b_1}$, $\mathbf{b_2}$ are also $(N \times 1)$ vectors containing the values of the fictitious loads at the nodal points and $\mathbf{x}_k = \{x_1^k, x_2^k, \ldots, x_N^k\}^{\mathrm{T}}$ are vectors containing the kth power of the abscissas of the nodal points.

Finally, collocating Eqs. (23) and (24) at the N nodal points and substituting the derivatives from Eqs. (59)–(66) yields the following system of equations:

$$\mathbf{M}_{11}\ddot{\mathbf{c}}_1 + \mathbf{M}_{12}\ddot{\mathbf{b}}_1 - \mathbf{K}_1(\mathbf{b}_1, \mathbf{b}_2, \mathbf{c}_1, \mathbf{c}_2) = \mathbf{p}_x, \tag{67}$$

$$\mathbf{M}_{21}\ddot{\mathbf{c}}_2 + \mathbf{M}_{22}\ddot{\mathbf{b}}_2 - \mathbf{K}_2(\mathbf{b}_1, \mathbf{b}_2, \mathbf{c}_1, \mathbf{c}_2) = \mathbf{p}_z, \tag{68}$$

where $\mathbf{M}_{ij}$ are known generalized mass matrices; $\mathbf{K}_i(\mathbf{b}_1, \mathbf{b}_2, \mathbf{c}_1, \mathbf{c}_2)$ generalized stiffness vectors and $\mathbf{c}_1 = \{c_1, c_2\}^{\mathrm{T}}$, $\mathbf{c}_2 = \{c_3, c_4, c_5, c_6\}^{\mathrm{T}}$. Eqs. (67) and (68) constitute a system of $2N$ equations of motion with $2N + 6$ unknowns. The required six additional equations result from the boundary conditions. Thus, after substituting the relevant derivatives into Eqs. (25)–(30), one obtains

$$\mathbf{f}(\mathbf{b}_1, \mathbf{b}_2, \mathbf{c}_1, \mathbf{c}_2) = \mathbf{0}, \quad i = 1, 2, \ldots, 6. \tag{69}$$

Eqs. (69) play the role of six constraints, in general non-linear, for the $2N + 6$ generalized co-ordinates $\mathbf{b}_1, \mathbf{b}_2, \mathbf{c}_1, \mathbf{c}_2$. They can be used to eliminate $\mathbf{c}_1$, $\mathbf{c}_2$ from Eqs. (67) and (68). The elimination procedure is highly simplified if the inertia force $\rho\ddot{u}$ is neglected. In this case the terms $\mathbf{M}_{11}\ddot{\mathbf{c}}_1$ and $\mathbf{M}_{12}\ddot{\mathbf{b}}_1$ are dropped from Eqs. (67) and the boundary conditions (69) become linear with respect to $\mathbf{c}_1$, $\mathbf{c}_2$. This leads to the following equations of motion:

$$\mathbf{K}_1(\mathbf{b}_1, \mathbf{b}_2, \mathbf{c}) = \mathbf{p}_x, \tag{70}$$

$$\mathbf{M}\ddot{\mathbf{b}}_2 - \mathbf{K}_2(\mathbf{b}_1, \mathbf{b}_2, \mathbf{c}) = \mathbf{p}_z(t), \tag{71}$$

where $\mathbf{M}$ is the known $(N \times N)$ generalized mass matrix; $\mathbf{K}_i(\mathbf{b}_1, \mathbf{b}_2, \mathbf{c})$ generalized stiffness vectors and $\mathbf{c} = \{c_1, c_2, \ldots, c_6\}^{\mathrm{T}}$. The boundary conditions (69) are now written as

$$\mathbf{f}(\mathbf{b}_1, \mathbf{b}_2, \mathbf{c}) = \mathbf{0}. \tag{72}$$

Eq. (71) is the semi-discretized equation of motion of the beam. The associated initial conditions result from Eq. (62) when combined with Eqs. (33) and (34). This gives

$$\mathbf{b}_2(0) = \mathbf{G}_2^{-1}(\tilde{\mathbf{w}}_0 - c_3\mathbf{x}_3 - c_4\mathbf{x}_2 - c_5\mathbf{x}_1 - c_6\mathbf{x}_0), \tag{73}$$

$$\dot{\mathbf{b}}_2(0) = \mathbf{G}_2^{-1}\dot{\tilde{\mathbf{w}}}_0. \tag{74}$$

The time step integration method for non-linear equations of motion can be employed to solve Eq. (71). In each iteration for $\mathbf{b}_2$ within a time step, the current value of $\mathbf{b}_2$ is utilized to update the vectors $\mathbf{b}_1$ and $\mathbf{c}$ on the basis of Eqs. (70) and (72). This demands the solution of a non-linear system of algebraic equations, which is performed using the modified Newton–Raphson method. In this paper, the average acceleration time step integration method was employed to solve Eq. (71) and the results were cross-checked by a time step integration method based on the analog equation method [16]. Once the vectors $\mathbf{b}_1, \mathbf{b}_2, \mathbf{c}$ are computed the displacement vectors $\mathbf{u}$, $\mathbf{w}$ and their derivatives at any instant t are evaluated from Eqs. (59)–(66).

3.1. Treatment of discontinuities

a. If the loading is discontinuous at a nodal point, the mean value can be employed to restore the continuity. The results are highly improved by adjusting the smoothing curve e.g. (see Fig. 3a)

$$p(x) = \frac{p_1 + p_2}{2} + \frac{p_2 - p_1}{2}\sin\frac{\pi(x - x_0)}{2\varepsilon}, \quad x_0 - \varepsilon \leqslant x \leqslant \varepsilon + x_0. \tag{75}$$

b. The concentrated force P at a point $x = x_0$ can be represented by a bell-shaped continuous function extended on a small region of length 2ε e.g. (see Fig. 3b)

$$p(x) = \frac{P}{2\varepsilon}\left[1 + \cos\frac{\pi(x - x_0)}{2\varepsilon}\right], \quad x_0 - \varepsilon \leqslant x \leqslant \varepsilon + x_0, \tag{76}$$

where

$$\int_{x_0-\varepsilon}^{x_0+\varepsilon} p(x)\,\mathrm{d}x = P. \tag{77}$$

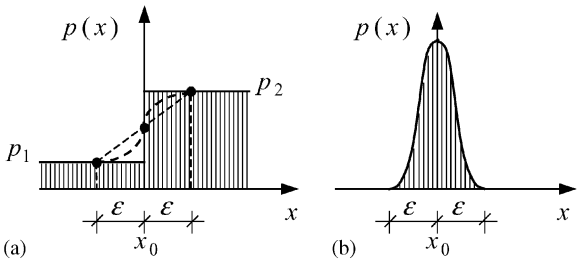

Fig. 3.

4. Numerical examples

On the base of the procedure described in previous section a FORTRAN program has been written for the non-linear dynamic analysis of beams with arbitrarily varying stiffness. In all examples the results have been obtained on a Pentium III PC and a few milliseconds were required for each time step to get accurate results using only $N = 21$ nodal points along the beam.

4.1. Uniform cross-section. Free vibrations

For the comparison of the results with those available from the literature, the free vibrations of a beam with uniform rectangular cross-section $b \times h$ and length $l = 1.0$ m have been studied. The employed data are $E = 2.1 \times 10^8$ kN/m^2, $b = 0.01$ m, $h = 0.03$ m and $\rho = 2355$ kg/m. Three types of boundary conditions are considered (i) hinged–hinged, (ii) fixed–hinged and (iii) fixed–fixed. The employed initial conditions are $\tilde{w}(x) = 16w_0(\xi^4 - 2\xi^3 + \xi)/5$, $\tilde{w}(x) = 4w_0(2\xi^4 - 5\xi^3 + 3\xi^2)$, $\tilde{w}(x) = 16w_0(\xi^4 - 2\xi^3 + \xi^2)$, respectively; $\xi = x/l$ and w_0 is the central deflection of the beam. In all three cases it is assumed $\dot{\tilde{w}}(x) = 0$. In Table 1 results for the frequency ratios ω_0/ω at various amplitude ratios w_0/ζ are presented compared with existing solutions; ω_0 is the respective frequency of the linear vibration and $\zeta = \sqrt{I/A}$ is the radius of gyration.

4.2. Uniform cross-section. Concentrated load

A fixed–fixed beam with uniform rectangular cross-section $b \times h$ and length $l = 0.508$ m has been analyzed under a suddenly applied concentrated force of $P = 2.844$ kN ($t \geqslant 0$) acting at the midspan of the beam with zero initial conditions. The employed data are: $E = 2.07 \times 10^8$ kN/m^2, $b = 0.0254$ m, $h = 0.003175$ m and $\rho = 0.2186$ kg/m. Many investigators have studied this problem. McNamara [11] used five beam bending elements based on a central-difference operator, Mondkar and Powell [12] used five eight-node plane stress elements to model one-half of the beam, Yang and Saigal [13] used six beam elements and Leung and Mao [14] used six beam elements for the one-half of the beam. The time history of the central deflection is shown in Fig. 4. In Table 2 the maximum deflection and the period of the first cycle are presented as compared with the solutions given in the above references. The obtained results are closer to those given in Refs. [12] and [13], which according to our opinion are the most accurate.

Table 1
Frequency ratios ω_0/ω at various amplitude ratios w_0/ζ in Example 4.1

w_0/ζ	Hinged–hinged			Fixed–hinged			Fixed–fixed		
	AEM	Ref. [9]	Ref. [14]	AEM	Ref. [9]	Ref. [14]	AEM	Ref. [9]	Ref. [14]
0.2	1.003	1.004	1.004	1.003	1.002	1.002	1.002	1.001	1.001
0.6	1.032	1.033	1.036	1.019	1.017	1.021	1.008	1.008	1.011
1.0	1.089	1.089	1.070	1.052	1.047	1.057	1.021	1.022	1.030
3.0	1.623	1.626	1.673	1.364	1.362	1.416	1.179	1.183	1.322
5.0	2.347	2.350	2.350	1.815	1.829	1.916	1.429	1.447	1.556

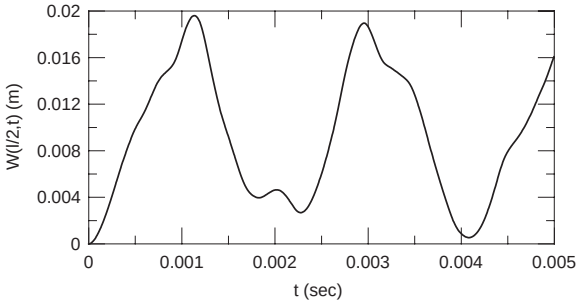

Fig. 4. Time history of the central deflection of Example 4.2.

Table 2
Maximum deflection $w_{\max}$ (m) and period T (μs) of the first cycle in Example 4.2

	AEM	Ref. [11]	Ref. [12]	Ref. [13]	Ref. [14]
$w_{\max}$ (m)	0.01960	0.02286	0.01956	0.01956	0.01946
T (μs)	2275	2884	2300	2300	2151

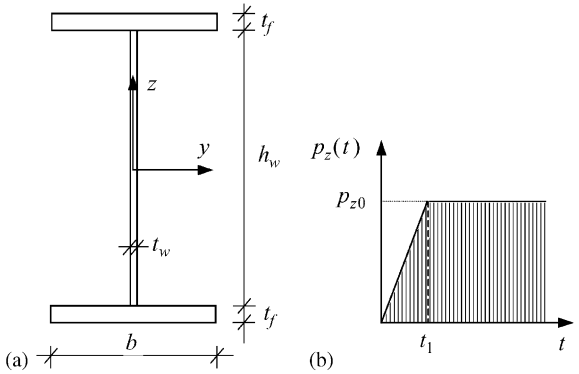

Fig. 5. (a) Cross-section of the steel I-section beam, (b) load history of the "static" load.

4.3. Uniform cross-section. Distributed load

The forced vibrations of a steel I-section beam with length $l = 10.0$ m have been studied using both theories referred to as deformed and undeformed configuration. The cross-section is constructed from a pair of identical flange plates $b = 300$ mm wide by $t_f = 30$ mm thick and a web plate $t_w = 12$ mm thick with height $h_w = 500$ mm (see Fig. 5a). The other data are: $E = 2.1 \times 10^8$ kN/m^2, $\rho = 188.40$ kg/m. The applied dynamic load is the so-called "static" load $p_z(t) = p_{z0}t/t_1$ if $0 \leqslant t \leqslant t_1$ and $p_z(t) = p_{z0}$ if $t_1 \leqslant t$ ($t_1 = 0.02$ s) with zero initial conditions (see Fig. 5b). The examined boundary conditions are depicted in Fig. 6. The load $p_{z0} = 3000$ kN/m was used except from the last case where it was taken $p_{z0} = 300$ kN/m. The time histories of the displacements u and w are shown in Figs. 7–13 at the cross-section $x_0 = 6.9048$ m. From these

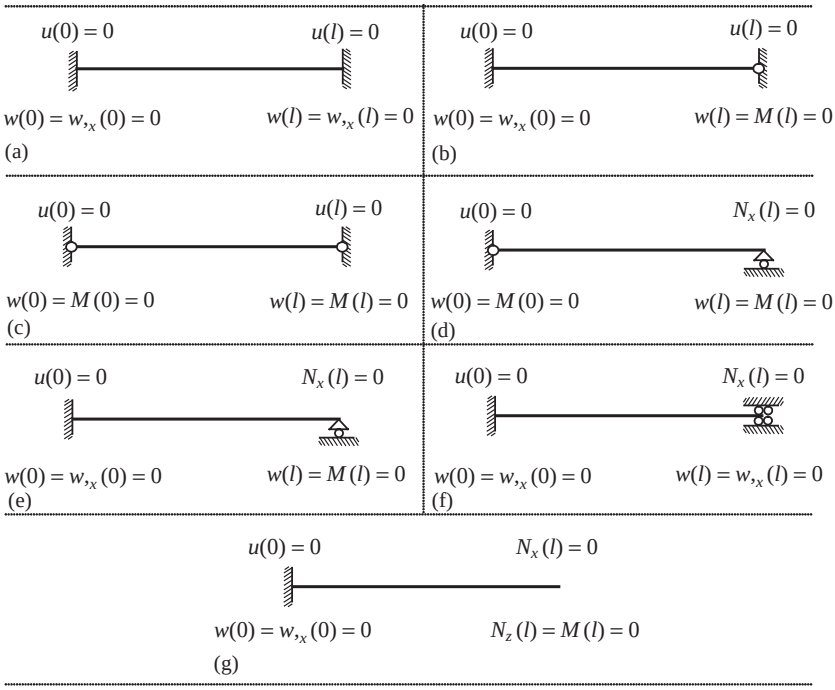

Fig. 6. Boundary conditions in Example 4.3.

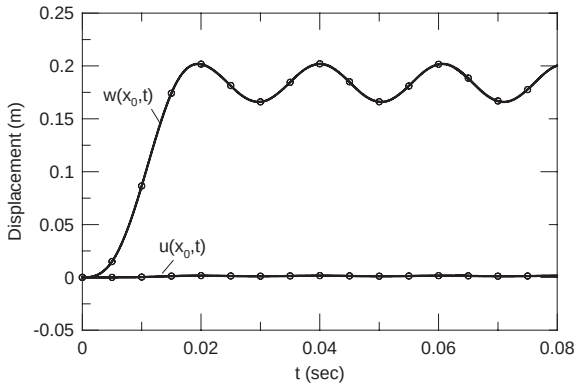

Fig. 7. Time history of the displacements in Example 4.3. Boundary conditions: Case (a) ——, deformed configuration; —○—, undeformed configuration.

figures one can conclude that for axially immovable ends the deviation between the two sets of governing equations is negligible (see Figs. 7–9). However, for axially movable ends the deviation may be appreciable (see Figs. 10–13). The same conclusion can be drawn from the time history of the ratio $Qw_{,x}/N$. That is, the ratio $Qw_{,x}/N$ for fixed–fixed ends is small (see Fig. 14), while for pinned-roller ends this ratio approaches the value of 1 as it was anticipated (see Fig. 15).

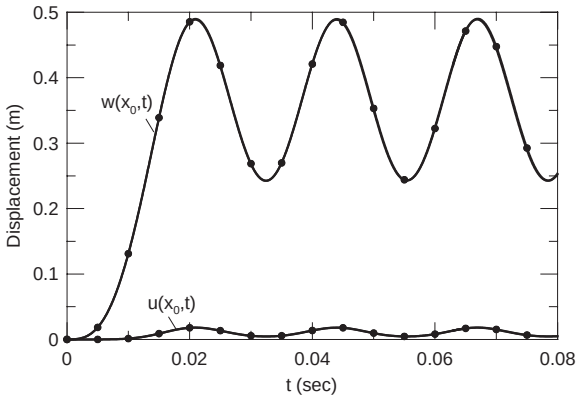

Fig. 8. Time history of the displacements in Example 4.3. Boundary conditions: Case (b). ——, deformed configuration; —○—, undeformed configuration.

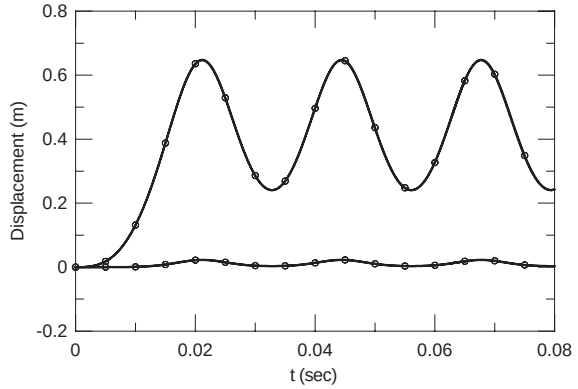

Fig. 9. Time history of the displacements in Example 4.3. Boundary conditions: Case (c). ——, deformed configuration; —○—, undeformed configuration.

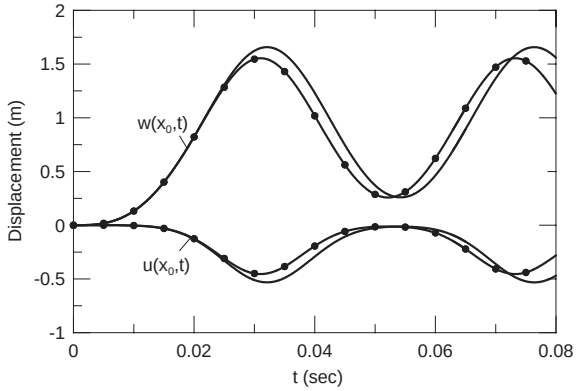

Fig. 10. Time history of the displacements in Example 4.3. Boundary conditions: Case (d). ——, deformed configuration; —○—, undeformed configuration.

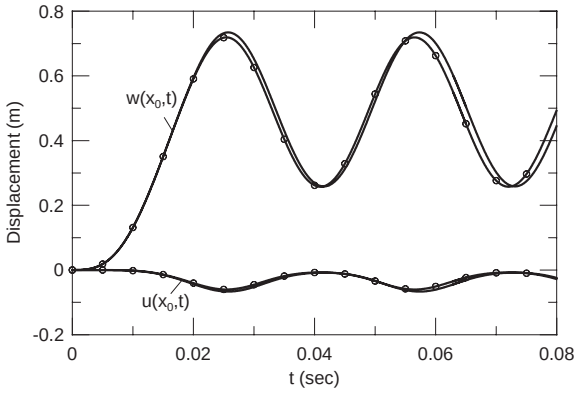

Fig. 11. Time history of the displacements in Example 4.3. Boundary conditions: Case (e). ——, deformed configuration; —◦—, undeformed configuration.

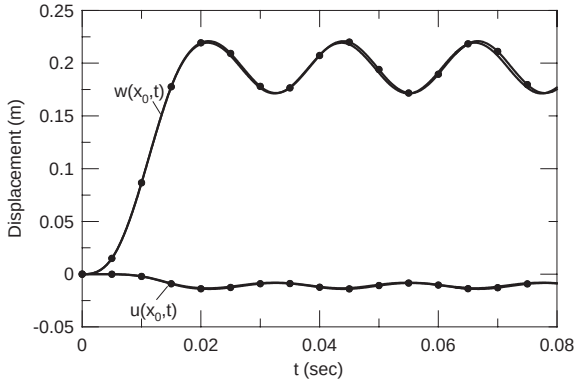

Fig. 12. Time history of the displacements in Example 4.3. Boundary conditions: Case (f). ——, deformed configuration; —◦—, undeformed configuration.

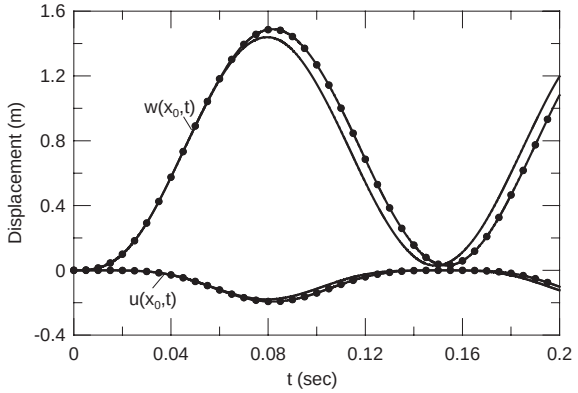

Fig. 13. Time history of the displacements in Example 4.3. Boundary conditions: Case (g). ——, deformed configuration; —◦—, undeformed configuration.

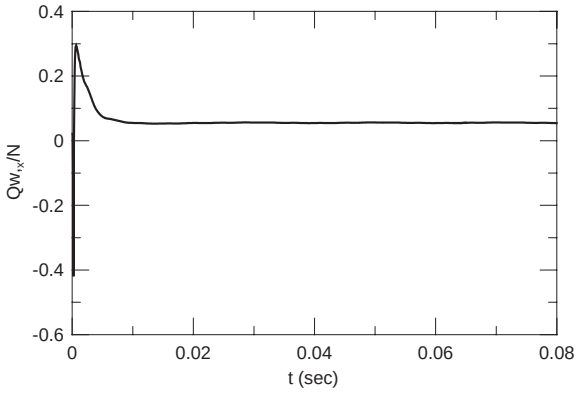

Fig. 14. Time history of the ratio $Qw_{,x}/N$ in Example 4.3. Boundary conditions: Case (a).

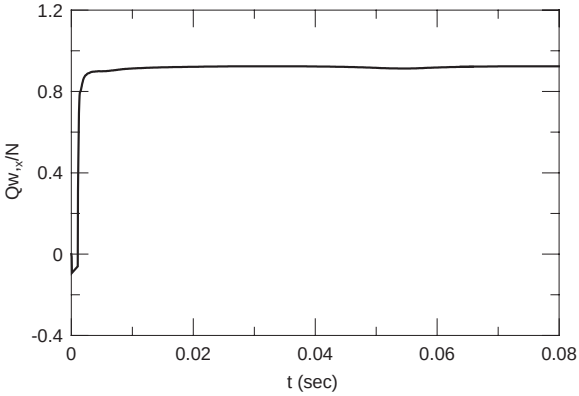

Fig. 15. Time history of the ratio $Qw_{,x}/N$ in Example 4.3. Boundary conditions: Case (d).

4.4. Variable cross-section. Free and forced vibrations

The free and forced vibrations of the steel I-section beam of Example 4.3 have been studied under varying web height $h_w(x)$. Two cases are considered: (a) constant web height, $h_w = h_w(0)$ and (b) linearly varying web height, $h_w = h_w(0)(0.5 + x/l)$. In both cases the volume of the material, i.e., $V = [t_w h_w(0) + 2t_f b]l$, was kept constant. The mass density per unit length is $\rho = 7850A(x)$ kg/m.

Three types of boundary conditions are considered (i) hinged–hinged, (ii) fixed–hinged and (iii) fixed–fixed. In Figs. 16 and 17 results for the natural vibrations are presented for cases (a) and (b), respectively. The employed initial conditions were those of Example 4.1 ($w_0 = 1.0$ m). In Fig. 18, the dependence of the period T (T_0 is the period of the linear vibration) on the maximum amplitude is shown for both cases. Finally, the forced vibrations have been studied under the "static" load ($p_{z0} = 3000$ kN/m, $t_1 = 0.02$ s) with zero initial conditions. The time histories of the central deflection for cases (a) and (b) are shown in Figs. 19 and 20 respectively.

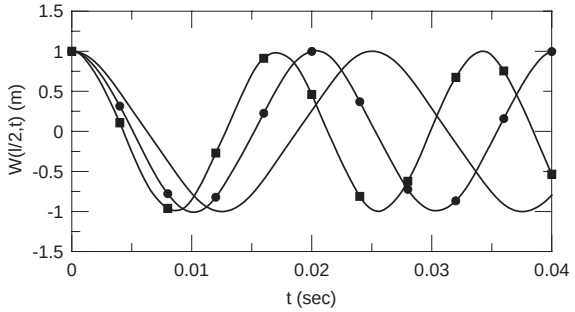

Fig. 16. Free vibrations in Example 4.4. Time history of the central deflection: Case (a). ——, BCs hinged–hinged; —●—, BCs fixed–hinged; —▩—, BCs fixed–fixed.

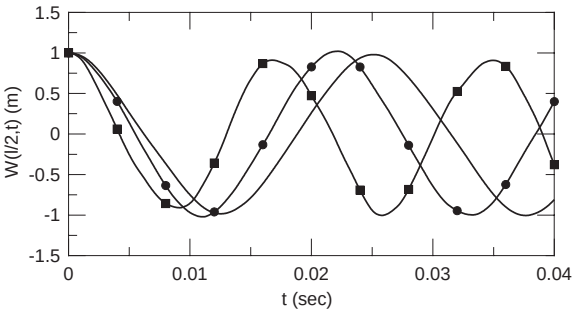

Fig. 17. Free vibrations in Example 4.4. Time history of the central deflection: Case (b). ——, BCs hinged–hinged; —●—, BCs fixed–hinged; —▩—, BCs fixed–fixed.

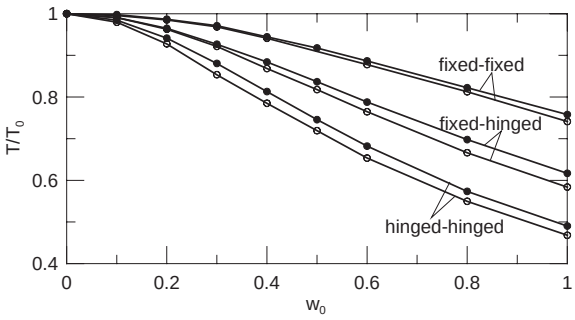

Fig. 18. Period versus maximum amplitude in Example 4.4. —●—, case (a); —○—, case (b).

5. Conclusions

In this paper a direct solution to dynamic problem of beams with variable stiffness undergoing large deflections has been presented. The governing equations have been derived considering the dynamic equilibrium in the deformed configuration. The presented solution is based on the concept of the analog equation, which converts the two coupled non-linear equations of motion

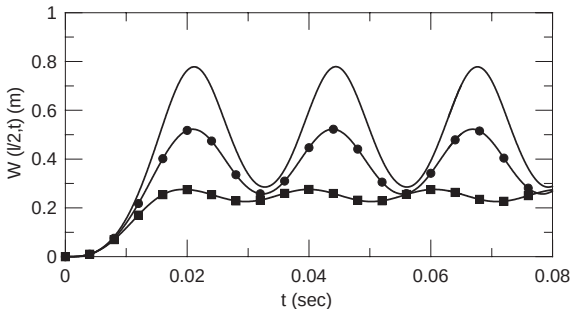

Fig. 19. Forced vibrations in Example 4.4. Time history of the central deflection: Case (a). ——, BCs hinged–hinged; —●—, BCs fixed–hinged; —▩—, BCs fixed–fixed.

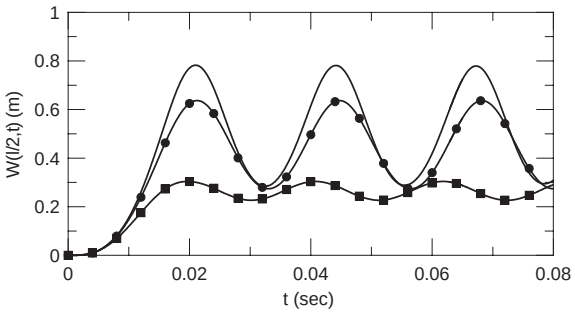

Fig. 20. Forced vibrations in Example 4.4. Time history of the central deflection: Case (b). ——, BCs hinged–hinged; —●—, BCs fixed–hinged; —▩—, BCs fixed–fixed.

into two quasi-static uncoupled linear equations with fictitious loads. These equations are subsequently solved using the one-dimensional integral equation method. From the presented analysis and the numerical examples the following main conclusions can be drawn.

(a) Only simple fundamental solutions pertaining to the static problem are employed to derive the integral representation of the solution.
(b) The displacements and the stress resultants are computed at any point using the respective integral representation as a mathematical formula.
(c) Accurate numerical results for the displacements and the stress resultants are obtained.
(d) The solution of the static problem can be obtained using the same computer program if the inertia forces are neglected.
(e) The influence of the shear force on the axial force may be appreciable in the case of axially movable ends. Therefore inaccuracies may result, if the response of the system is obtained using the simplified equations resulting from the equilibrium of the undeformed element.
(f) Beam structures can be also analyzed using the beam as substructure avoiding, thus, fine FEM discretizations within each beam. A requirement that is more pronounced for beams with variable stiffness.

References

[1] S. Woinowsky-Krieger, The effects of an axial force on the vibration of hinged bars, *Transactions of the ASME* 72 (1950) 35–36.
[2] D.A. Evensen, Nonlinear vibrations of beams with various boundary conditions, *American Institute of Aeronautics and Astronautics Journal* 6 (1968) 370–372.
[3] A.V. Srinivasan, Large amplitude free oscillations of beams and plates, *American Institute of Aeronautics and Astronautics Journal* 3 (1965) 1951–1953.
[4] J.D. Ray, C.W. Bert, Nonlinear vibration of a beam with pinned ends, Transactions of the American Society of Mechanical Engineers, *Journal of Engineering for Industry* 91 (1969) 997–1004.
[5] L.S. Raju, G.V. Rao, K.K. Raju, Large amplitude free vibrations of tapered beams, *American Institute of Aeronautics and Astronautics Journal* 14 (1976) 280–282.
[6] H. Sato, Non-linear free vibrations of stepped thickness beams, *Journal of Sound and Vibration* 72 (1980) 415–422.
[7] N.S. Abhyankar, E.K. Hall, S.V. Hanagud, Chaotic vibrations of beams: numerical solutions of partial differential equations, *Journal of Applied Mechanics* 60 (1993) 167–174.
[8] G.R. Bhashyam, G. Prathap, Galerkin finite element method for non-linear beam vibrations, *Journal of Sound and Vibration* 72 (1980) 191–203.
[9] G. Singh, G.V. Rao, N.G. Iyengar, Re-investigation of large amplitude free vibrations of beams using finite elements, *Journal of Sound and Vibration* 143 (1990) 351–355.
[10] K.K. Raju, B.P. Shastry, G.V. Rao, A finite element formulation for the large amplitude vibrations of tapered beams, *Journal of Sound and Vibration* 47 (1976) 595–598.
[11] J.E. McNamara, Solution schemes for problems of nonlinear structural dynamics, *Journal of Pressure Vessel Technology, American Society of Mechanical Engineers* 96 (1974) 96–102.
[12] D.P. Mondkar, G.H. Powell, Finite element analysis of nonlinear static and dynamic response, *International Journal for Numerical Methods in Engineering* 11 (1977) 499–520.
[13] T.Y. Yang, S. Saigal, A simple element for static and dynamic response of beams with material and geometric nonlinearities, *International Journal for Numerical Methods in Engineering* 20 (1984) 851–867.
[14] A.Y.T. Leung, S.G. Mao, Symplectic integration of an accurate beam finite element in non-linear vibration, *Computers & Structures* 54 (1995) 1135–1147.
[15] J.T. Katsikadelis, The analog equation method—a powerful BEM-based solution technique for solving linear and nonlinear engineering problems, in: C.A. Brebbia (Ed.), *Boundary Elements XVI*, CLM Publications, Southampton, 1994, pp. 167–182.
[16] J.T. Katsikadelis, A new time step integration scheme for structural dynamics based on the analog equation method, in: *Collection of Papers Dedicated to Prof. P.S. Theocaris*, National Technical University of Athens, 1994, pp. 80–100.